Solvent-controlled reversible switching between adsorbed self-assembled nanoribbons and nanotubes

Asad Jamal, Irina Nyrkova, Philippe Mesini, Swann Militzer, Günter Reiter

Solvent-controlled reversible switching between adsorbed self-assembled nanoribbons and nanotubes

Asad Jamal[ab], Irina Nyrkova[c], Philippe Mesini[c], Swann Militzer[c] and Günter Reiter[ab]*

[a] Institute of Physics, University of Freiburg, Herman-Herder-Strasse 3, 79104 Freiburg, Germany

[b] Freiburg Materials Research Center (FMF), University of Freiburg, Stefan-Meier-Strasse 21, 79104 Freiburg, Germany

[c] Institut Charles Sadron, 23 rue du Loess BP 84047, F- 67034 Strasbourg Cedex 2, France

Email: guenter.reiter@physik.uni-freiburg.de

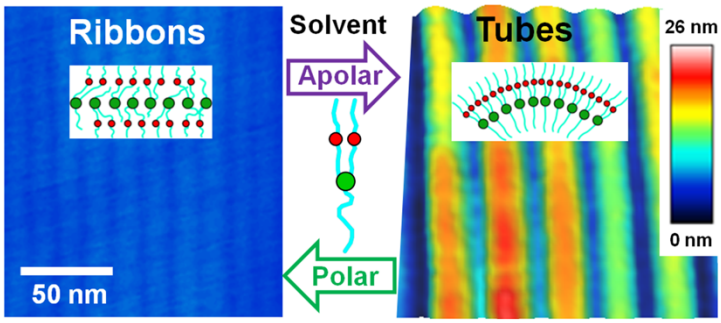

ABSTRACT

We have demonstrated that solutions of 3,5-bis-(5-hexylcarbamoylpentyloxy)-benzoic acid decyl ester (BHPB-10) can form metastable nanostructures on solid substrates and in the bulk. BHPB-10 is an achiral molecule involving several distinct, strongly interacting groups (SIGs), one aromatic-ester ring and two amide groups per a molecule. Specific

solvents affect interactions between particular SIGs, thus promoting various nano-structures: lamellae, nanoribbons, helical ribbons, or nanotubes. In cyclohexane, a solvent allowing for both inter-amide hydrogen bonds and mutual attraction of rings, formation of nanotubes with a diameter of 28 ± 5 nm was observed in the bulk and on surfaces. By contrast, in cyclohexanone, which suppresses inter-amide hydrogen bonds, flat nanoribbons with specific width of 12 ± 4 nm were formed on solid substrates after drying. By annealing in cyclohexane vapor, we followed the process of switching surface structures from nanoribbons to nanotubes and observed helical ribbons as the precursor of nanotubes. We also turned nanotubes back into nanoribbons by adding cyclohexanone, thus demonstrating reversible switching along the route: tubes → lamellae → flat ribbons → helical ribbons → tubes. We propose models explaining the observed nanostructures and their transformations, including the origin of spontaneous chirality of the helical ribbons. Our findings for the self-assembly in the achiral BHPB-10 solutions provide insight in the influence of complementary inter-molecular specific SIG-based interactions and demonstrate an effective pathway for tailoring the shape and size of nanostructures derived from the same building unit.

KEYWORDS: metastable nanostructures, surface self-assembling, solvent vapor annealing, strongly interacting group (SIG), spontaneous chirality

Introduction

Self-assembly is a key approach in nanotechnology, which provides a route for controlled structure formation in a bottom up approach.[1–5] Building blocks spontaneously producing

tubular morphologies[5–7] are relatively rare. However, nanotubes are of special interest because of diverse potential applications, which range from high tensile strength materials[8] to tissue engineering[9], from catalysis[10] to drug delivery[11,12], from electronic and magnetic devices[13] to nanolasers, waveguides and quantum dots[14,15], from biosensors[16–18] to transmembrane ion transport in biological systems[19–21]; tubes can also be used for nanolithography, as template or cortex for nanowires, nanocylinders or fibrils.[22–26] For many of these applications the control of size and size distribution of the tubes are formidable issues.[27] In particular, tubes of monodisperse width are formed in solutions, involving twisted structures, which are the result of an interplay between the internal helicity of the building blocks and elastic or surface stabilizing forces.[7,19] For many (e.g., optoelectronic) applications an important goal is the formation of ordered long-ranged two-dimensional structures made of tubes. However, in contrast to direct formation on surfaces, sedimentation of long rigid objects from solutions usually results in kinetically frozen, non-ordered or fragmented deposits,[1,7,27].

Self-assembly of molecules into helical or tubular structures can be controlled by parameters like concentration, temperature or solvent composition.[28,29] These parameters affect directly or indirectly interactions between molecules. In addition, properties of molecules like their shape, rigidity, charges, chirality or, in case of amphiphilic molecules, the volume ratio of their hydrophilic and hydrophobic parts may have an impact on the formation of helical or tubular structure.[27,30–33] So far, it was often assumed that the building blocks or the solvent have to be chiral in order to obtain helical or tubular structures.[34–39] However, there are a few studies,[40–43] which report the formation of helical supramolecular structures in achiral systems. In these systems, the induction of

chirality in the resulting nanostructures was attributed to symmetry breaking phenomena with respect to molecular tilt or conformation. In a recent study, Wang et al.[44] have demonstrated the formation of a collection of alternative structures (like nanotubes, helical ribbons, stripes and membranes) in solutions of achiral azobenzene-based molecules, which are capable of performing a reversible cis-trans transformation. As cis-conformations result in chiral centers within these molecules, such symmetry breaking may induce chiral structures. The resulting morphology depended on the incubation temperature. However, Wang et al. did not propose a model for local chiral supramolecular organization within these nanostructures. In addition, the structures observed in ref. 44, even after 2 months of equilibration, were rather defective, short in lengths, suggesting that they have not yet reached equilibrium. Although the exact mechanism responsible for the formation of chiral nanostructures in achiral systems is still a matter of debate,[45–48] these previous studies have clearly demonstrated that chiral nanostructures can be realized via self-assembly of achiral molecules.

The family of aromatic diamide esters, BHPB-*n* (Fig. 1), is a very convenient model system for studying helical and tubular structure formation in achiral systems. Indeed, BHPB-*n* can self-assemble in a range of organic solvents into various chiral nanostructures. In particular, tubes of various diameters can be formed depending on the tail length *n*.[49,50] All molecules from this family comprise two types of strongly interacting groups (SIGs), an aromatic-ester ring and two amide groups (polar parts). The presence of SIGs are known to alter the static and dynamic properties of diverse polymeric and oligomeric systems.[51–54] In BHPB-n family, both polar SIGs are connected to the aromatic ring via short spacers (C_5H_{10}) and decorated by various alkyl tails at its

three sides, as shown in Fig. 1.

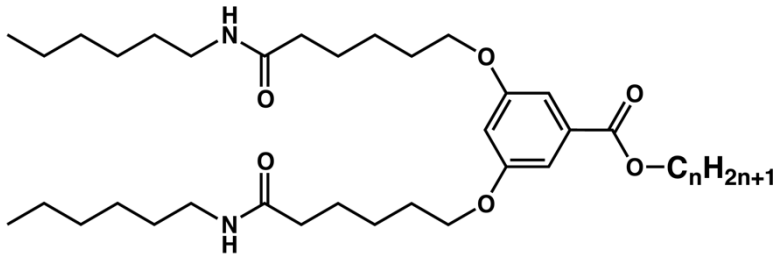

Fig. 1 Chemical structure of BHPB-n.

For the present study, we have chosen a member of this family, BHPB-10 (3,5-bis-(5-hexylcarbamoylpentyloxy)-benzoic acid decyl ester). Below, we focus on the formation and transformation of supramolecular nanostructures upon adsorption on a solid substrate. In particular, we aim to clarify the interplay of various directional molecular interactions and their importance for the formation of helical nanostructures in the achiral system under study. To this end, as the quality of the solvent has an influence on the interactions between the specific parts of BHPB-10 molecules, we study structure formation processes in BHPB-10 deposited from solutions of polar and apolar solvents. Using the same building unit, we show below how to control the pathways of structure formation and thereby to generate two morphologically different nanostructures, i.e., 2D supramolecular nanoribbons and 3D nanotubes. Furthermore, by changing the composition of the solvent, we could successfully switch between nanoribbons and nanotubes in a reversible manner.

Experimental Section

Sample preparation

Two solvents, cyclohexane and cyclohexanone, were used in our study to dissolve BHPB-10 molecules. Chemical structure of BHPB-10 is shown in Fig. 5a. At room temperature, the apolar cyclohexane is a poor solvent for BHPB-10.[49,50] Hence BHPB-10 suspensions (0.1 mg/ml) had to be heated at 60 °C for 6 h in order to achieve complete dissolution.[50] The solution was further diluted with hot solvent and finally cooled down to room temperature. By contrast, cyclohexanone, being a polar solvent, is a good solvent for BHPB-10, even at room temperature. Thus, complete dissolution of the molecules was obtained at room temperature. The dissociation of aggregates of BHPB-10 in cyclohexane can be detected by DSC, which shows an endothermic peak at 47 °C for concentration of 0.1 wt. %, indicating a first order phase transition from aggregates to homogeneously dissolved BHPB-10. In the course of 24 hours at room temperature, the viscosity of cyclohexane solutions increased while cyclohexanone based solution showed a low viscosity, independent of time.

As substrates, we used Si wafers, which we cut into 1×1 cm^2 pieces. Before use, these substrates were cleaned with acetone in an ultrasonic bath for 15 min, rinsed with ethanol and then with distilled water. These substrates were finally blown dry in a stream of nitrogen gas. For cyclohexane solutions, samples were prepared by depositing 5 µl of BHPB-10 solutions at room temperature via spin coating (at 800 rpm). For cyclohexanone solutions, we deposited the molecules via drop casting and dried the samples in an oven at 25 °C for 14 hours, followed by 2 hours in vacuum at 150 mbar. Temperature enhanced solvent vapor annealing (TESVA) is an attractive option for tuning and equilibrating self-assembled structures on the surfaces. Temperature can

provide mobility to the molecules and solvent can be used to tune the interactions between them. In a closed chamber kept at the desired temperature and saturated with solvent vapor , the molecules deposited on the substrate or within nanostructures may gain mobility and thus could re-order according to the forces acting between them.[55–57] For this reason, we annealed samples prepared from cyclohexanone-based solutions in cyclohexane vapors by placing them in glass container closed with an airtight lid. This jar contained cyclohexane and was kept at 60 °C for different time intervals ranging from 30 minutes to 48 hours. Cyclohexane has a boiling point of ~81 °C. Thus, at 60 °C the closed jar (with a volume of 250 cm^3) was saturated with ~10^{14} molecules/cm^3. Accordingly, the BHPB-10 nanostructures were exposed to a large number of solvent molecules, which partially dissolved BHPB-10 structures on the substrate. The amount of cyclohexane molecules, which condensed onto the surface, was sufficient to enhance the mobility of BHPB-10 molecules, allowing them to rearrange on the surface.

Self-assembly is a reversible process. Therefore, nanostructures formed in cyclohexane can be dissolved when exposing them to a good solvent. Here, we dissolved self-assembled nanotubes formed in a cyclohexane solution (poor solvent) of BHPB-10 by exposure to cyclohexanone (good solvent). To this end, a cyclohexane solution was first heated to 65 °C. We then added the same amount (6 ml) of cyclohexanone and kept this mixed solution for 18 hours in open air at 65 °C. At this elevated temperature, as a consequence of the large difference in vapor pressure (p_{vap}) between cyclohexane (p_{vap} ≈ 612 mbar) and cyclohexanone (p_{vap} ≈ 1 mbar), cyclohexane evaporated much faster. After 18 hours, the solution contained only cyclohexanone and well-dissolved BHPB-10 molecules. This solution was cooled down to room temperature and kept there for about 5

hours before the samples on Si substrates were prepared by casting a 5 µl drop.

Characterization of surface morphology

Atomic force microscopy measurements (JPK, NANOWIZARD II) were performed in tapping mode in air at room temperature with soft cantilever sensors having a tip radius *r* < 10 nm, a resonance frequency of ~160 kHz and a spring constant (k) of ~7 N/m (Nanosensors). The typical scanning rate was 1 Hz. To investigate the mechanical properties of these nanotubes, measurements of the phase-signal from an individual nanotube were performed at different ratios (A/A_0) of set point amplitude (A) and free oscillation amplitude (A_0). The magnitude of the tapping force ($F = k(A_0 - A)$) increased with the decrease in A/A_0. For image analysis, image processing software from JPK and ImageJ were used.[58]

Results and Discussions

Self-assembled nanotubes and nanoribbons

Each BHPB-n molecule comprises two types of distinct sub-units, which may generate strong interactions between molecules: 1) Aromatic-ester rings are capable of mutual π-π interactions. 2) Amide groups provide the potential of mutual hydrogen bonding. In a neutral medium, such sub-units may segregate and hence act as SIGs which promote specific self-assembly processes.[53,59] The attached alkyl-chains improved solubility of the molecules but also introduced steric constraints, affecting the formation of nanostructures. Previous studies[49,50] showed that hydrogen bonding via the amide groups is of primary importance for self-assembling of BHPB-n molecules in appropriate solvents. Characteristic signatures in FTIR and UV spectra verified the formation of H-

bonds. The resulting aggregation, induced by changing temperature, caused changes in viscosity, but was also detectable in accompanying calorimetric measurements. Moreover, at room temperature in cyclohexane (a poor solvent for amide groups), all amide groups were involved in H-bonding.[49]

In the present study, we investigated structure formation favored by H-bonds between BHPB-10 molecules by comparing their behavior in two solvents, selected for providing different degrees of solubility of amide groups. Apolar cyclohexane stimulates aggregation because it favors H-bonds between amides. By contrast, polar cyclohexanone dissolves BHPB-10 molecules well, even at room temperature, because it competes with H-bond formation and hence can be considered as "inter-amide H-bond suppressor" (see FTIR spectra Fig. S-1 supporting these conclusions and the corresponding discussion in the ESM). In contrast to these differences with respect to the formation of H-bonds, both solvents favor formation of effective π-π interactions between the aromatic ester groups of BHPB-10.

In cyclohexane solutions at room temperatures at concentrations of 0.05 mg/ml or higher, BHPB-10 molecules were observed to form a self-supporting gel.[50] As a typical basic structural feature of this gel, nanotubes with a diameter of 20-30 nm were identified (cf. electron micrographs presented in references[49,50] and Fig. 2d). Based on atomic force microscopy (AFM) height measurements, we have confirmed the formation of nanotubes with such a diameter (see Fig. 2a-c). The values of the diameter of nanotubes measured via AFM have to be de-convoluted, taking into account the finite radius of curvature and the conical shape of the AFM tip (see Fig. 2f).

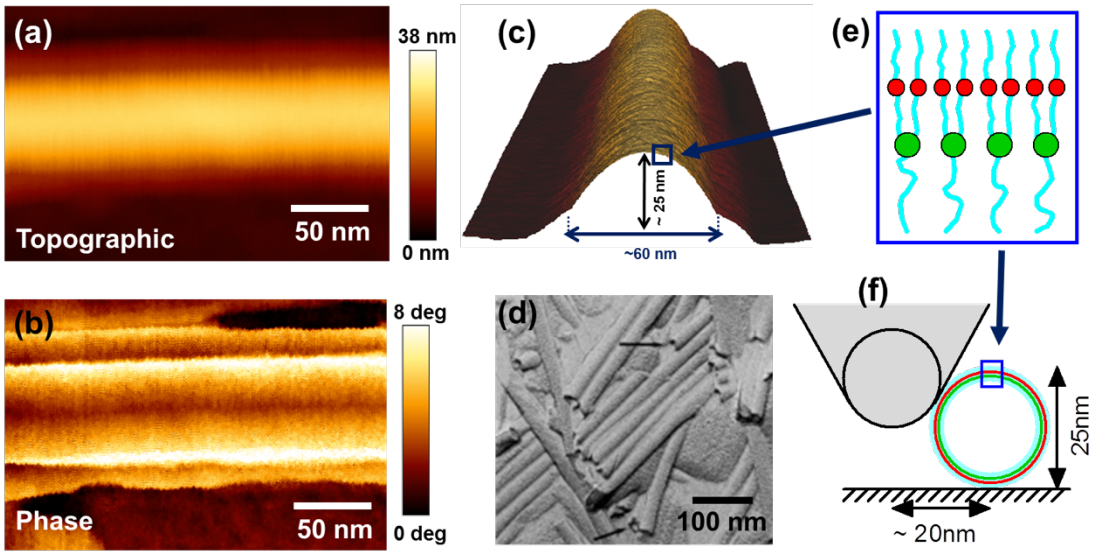

Fig. 2 AFM (a) topographic, (b) phase and (c) 3D phase images of BHBP-10 dissolved in cyclohexane (0.07 mg/ml) and deposited by spin-coating on a Si substrate showing the typical self-assembled tubular structures formed in solution. (d) Freeze fracture TEM of BHPB-10 gel in cyclohexane (15 mg/ml); arrows: cross-section of tube ends. (e) Scheme indicating the packing of molecules in a tubular structure (green and red circles represent the aromatic-ester and the amide units, respectively). (f) Schematic representations of an adsorbed nanotube and the cantilever near the surface. The width of the nanotube appears larger due to the gauges of the cantilever (its finite radius of curvature and its conical shape).

The AFM phase-signal images in Fig. 3a-d show the response of an individual nanotube to an increasing mechanical force (tapping force, F), applied via the AFM tip. With increasing F, the contrast in the phase-signal increased between the center and the periphery of the nanotube. The central part of the nanotube became darker than the periphery, indicating increased energy dissipation at the center. On the contrary, at the periphery of the nanotube showed only small changes in contrast, suggesting that the

walls of the nanotube were stiffer than the interior. We thus tentatively conclude that the nanotube was having a soft or empty interior surrounded by rather rigid walls. This hints at a hollow nanotube, consistent with previous electron microscopy results, Fig. 2d.

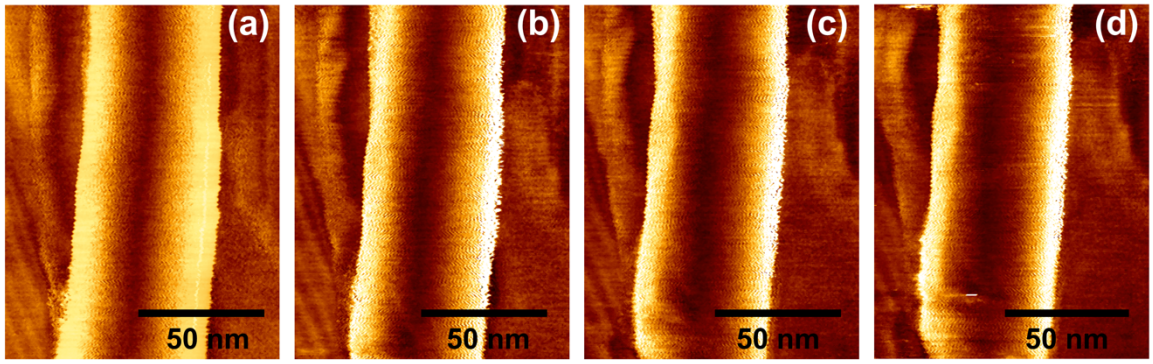

Fig. 3 AFM phase images of a nanotube measured at increasing tapping forces (F): (a) ~ 3 nN, (b) ~ 10 nN, (c) ~ 20 nN and (d) ~ 30 nN.

In cyclohexanone, a solvent suppressing the formation of H-bonds, we did not observe any aggregation of BHPB-10 or changes in the viscosity up to concentrations of 0.2 mg/ml. However, in the course of the drying process involved in the deposition onto solid substrates, the concentration of the solution increased to the level where nucleation and growth of ordered structure started, resulting in the formation of nanoribbons. To allow such ordering of BHPB-10 molecules during the drying process, samples were prepared by drop casting 5 μl of cyclohexanone solution of BHPB-10 on 1×1 cm^2 Si substrate resulting in a solution film having a thickness of ca. 50 μm. After complete evaporation of the solvent, AFM micrographs (Fig. 4a,b,c) showed well aligned self-assembled nanoribbons. Depending on the amount of BHPB-10 molecules deposited per unit area, monolayers or multilayers (for c > 0.05 mg/ml) of nanoribbons were formed on the Si-wafer. In each individual layer of a multilayer structure, all nanoribbons were oriented in

the same direction (Fig. 4c). The nanoribbons had a length of several micrometers and a typical width between 8 and 14 nm, with small gaps between adjacent nanoribbons. As shown in Fig. 4d, the height trace of Fig. 4c showed discrete steps in height with a value $h_1 \sim 3.2 \pm 0.7$ nm, which is apparently equal to the thickness of a monolayer. This value is consistent with the length of an elongated BHPB-10 molecule (Fig. 5a), indicating that each nanoribbon represents a single layer of molecules having their long axis oriented in the direction perpendicular to the surface.

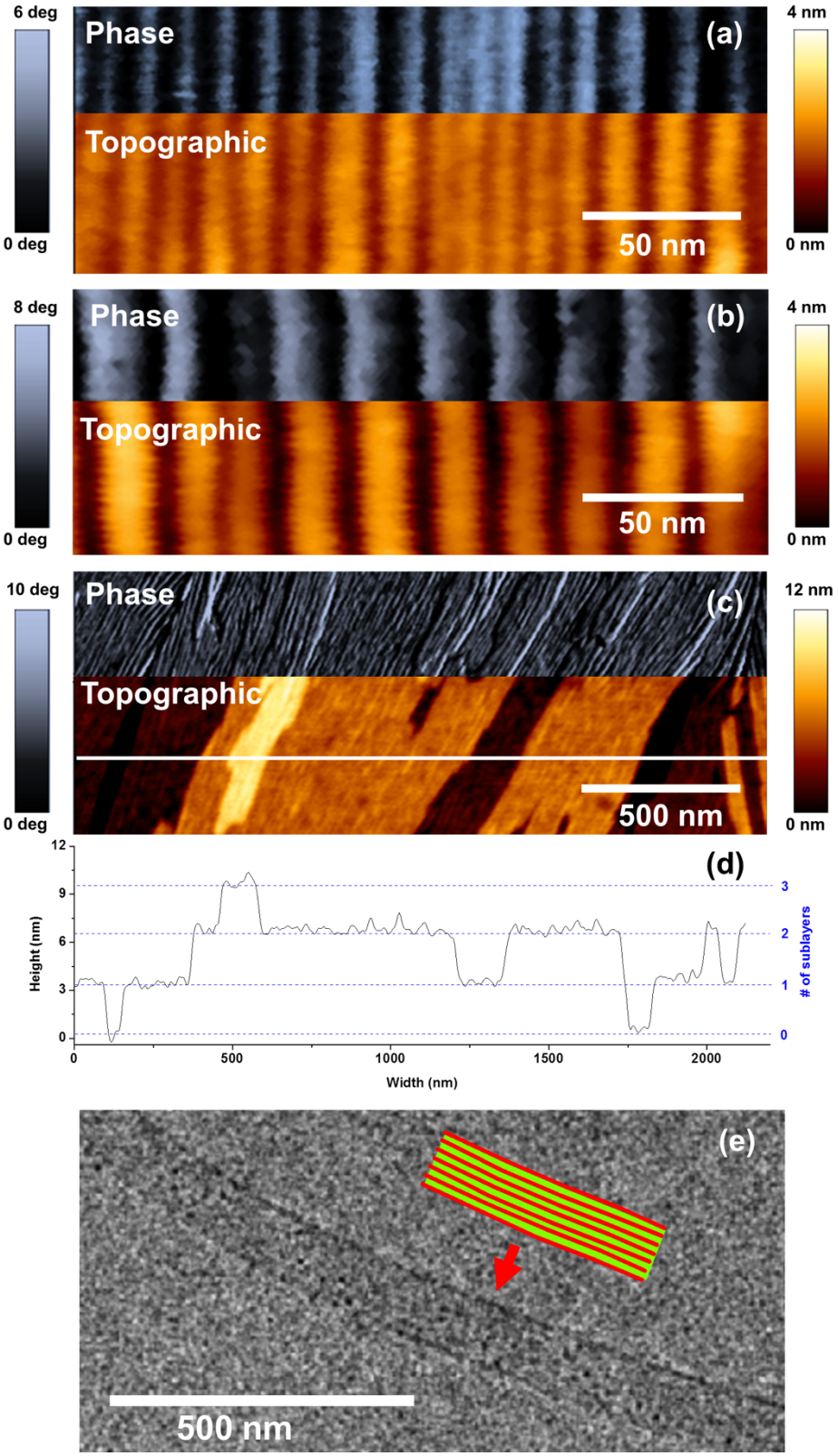
6 deg
0 deg
Phase
(a)
Topographic
50 nm
4 nm
0 nm
8 deg
0 deg
Phase
(b)
Topographic
50 nm
4 nm
0 nm
10 deg
0 deg
Phase
(c)
Topographic
500 nm
12 nm
0 nm
(d)
Height (nm)
# of sublayers
Width (nm)
0
500
1000
1500
2000
0
3
6
9
12
0
1
2
3
(e)
500 nm

Fig. 4 AFM images of the nanoribbons formed on Si wafers after drop casting of thin layers (ca. 50 μm) of cyclohexanone solutions of BHPB-10 with initial concentrations of: (a) 0.01 mg/ml (monolayer) and (b-c) 0.2 mg/ml (multilayer). Small-scale images (a,b) show nanoribbons all having similar widths. The large-scale image of the multilayered film (c) and its height profile (d) which shows discrete steps with a height corresponding to the length of an elongated BHPB-10 molecule; the total film height of the region consisting of three superposed layers was found to be 9.5 ± 1.5 nm. (e) TEM image of drop-casted cyclohexanone BHPB-10 solution (0.05 mg/ml) on a carbon coated grid (after tungsten coating of the dried deposit).

Mechanisms of molecular ordering and nano-structure formation in solvents of differing polarity

Self-assembly exploits properties of the solvent like its polarity or its protic/aprotic nature. These properties affect molecular interactions, *e.g.,* hydrogen bonding between self-assembling molecules, causing the formation of nanostructures of differing architectures.[60]

In cyclohexane, amide groups of BHPB-10 have a strong tendency for association via H-bonding. When inter-amide bonds are established, the aromatic-ester rings are restricted in mobility and hence are prone to mutual π-stacking. Hence, BHPB-10 molecules strongly interact via both, the amide and the aromatic types of meso-groups, which form separate parallel sub-layers (cf. IR and UV spectra in ref. 49, see also Fig. S-1 in the ESM). Molecular modeling (as in section S-5 in the ESM) shows that $C_{10}H_{21}$ alkyl tails are too long to be incorporated into the gaps between quasi-2D layers of amide

(red) and aromatic-ester (green) groups, which are covalently linked via short C_5H_{10} alkyl spacers (cf. Fig. 5a,c). Moreover, the $C_{10}H_{21}$ alkyl tails cannot cross the amide layers without destruction of their 2D-organization. This geometrical conflict can, however, be resolved if the $C_{10}H_{21}$ alkyl tails stay on one side of the ring layer while the amide groups form a 2D-sublayer on its other side (like in Fig. 2e, f), hence producing lamellar mesostructures with non-equivalent sides ("red-green sandwich" lamellas). Area mismatch between the amide (red) and the aromatic-ester (green) sub-layers leads to a tendency to spontaneous curvature of the sandwich lamella. Aromatic-ester groups prefer to stay parallel to each other in the ordered state. These π–π interactions prevent bending in the direction of these interactions because such bending would have cause a disruption of π–π interactions i.e., cost in free energy. As a consequence, only bending in the perpendicular direction (parallel to the π–stacked rings arranged into 2D crystalline or into 2D nematic sub-layer) is feasible (easy-bending direction). This fact prescribes a cylindrical shape for lamella, and hence a tubular meso-structure which eventually emerges in cyclohexane solutions of BHPB-10. The radius of the nanotubes formed by BHPB-n molecules increases with the length "n" of the alkyl tail (for tail lengths $8 \leq n \leq 12$, see section S-3 in ESM and ref. 49), this observation indicates that the amide layer is on the outer side of the nanotubes (as illustrated in Fig. 2f).

Contrary to cyclohexane, cyclohexanone is an inter-amide bond suppressor. Cyclohexanone has a ketone functional group, which strongly interacts via H-bonding with the amide groups in BHPB-10 (see Fig. S-1 in the ESM) and thus prevents their inter-amide stacking. The aromatic-ester SIGs have modest tendency to aggregation in cyclohexanone, hence they cannot produce structuring without extra aid at low BHPB-10

concentrations; this explains fluidity of such BHPB-10 solutions. In contrast to three dimensional bulk systems, in two dimensional systems additional interactions between surface and self-assembling molecules introduce a geometrical constraint on the growth of self-assembled structures, which can strongly influence and guide structure formation.[62–64] Given that molecules are adsorbed strongly, they are confined to the surface, i.e. their mobility in the direction away from the surface is restricted. However, molecules still can move in the lateral direction and rearrange within this confined space. As the concentration of BHPB-10 increases when the solvent evaporates during drop casting, BHPB-10 molecules come into close contact with each other, and the formation of π-π bonds between aromatic-ester rings of neighboring molecules becomes likely. Guided by the surface of the substrate, the rings join into 2D sub-layers parallel to the surface so that simple lamellar structures stabilized by ring SIGs are formed on the surface (note strong quadruple attractions between π-stacked objects[65,66]). In cyclohexanone solutions, no inter-amide structuring is established until, in the course of evaporation, almost no solvent is left. Before this last stage, the $C_{10}H_{21}$ tails mix with weakly ordered and strongly solvated amide groups on both sides of the ring sub-layers (one such lamella is shown in Fig. 5c). The strength of such solvation is demonstrated by the fact that residual cyclohexanone is observed (by FTIR spectra) in thin drop casted BHPB-10 films long way after their drying (the films are dried on touch in less than 15 minutes, however even 12 hours under high vacuum (1 mbar) is not enough to remove cyclohexanone completely, see Fig. S-2 and discussion in the ESM). Moreover, due to the presence of weak electric dipoles on the rings (cf. Fig. 5b) and due to the π-π nature of interactions within the corresponding sub-layer (the so-called 'parallel-displaced' π-π

mutual configuration of the rings is more stable than the 'sandwich' one[65]) an antiparallel arrangement of the aromatic-ester groups is more favorable. Therefore, we expect formation of a flat lamella with equivalent sides in highly concentrated (semi-dried) BHPB-10 solutions formed during the drop casting from cyclohexanone (see Fig. 5c) if the affinity of the alkyl chains to the substrate is strong enough (full damping of the surface). This is what can be seen from Fig. 4 where the wide (few hundred nm) strips of standard ~3.1 nm thickness (cf. AFM data in Fig. 4d and in the section S-2 in the ESM) are observed, see also the thinnest stripe-like aggregates visible by TEM, Fig. S-3b).

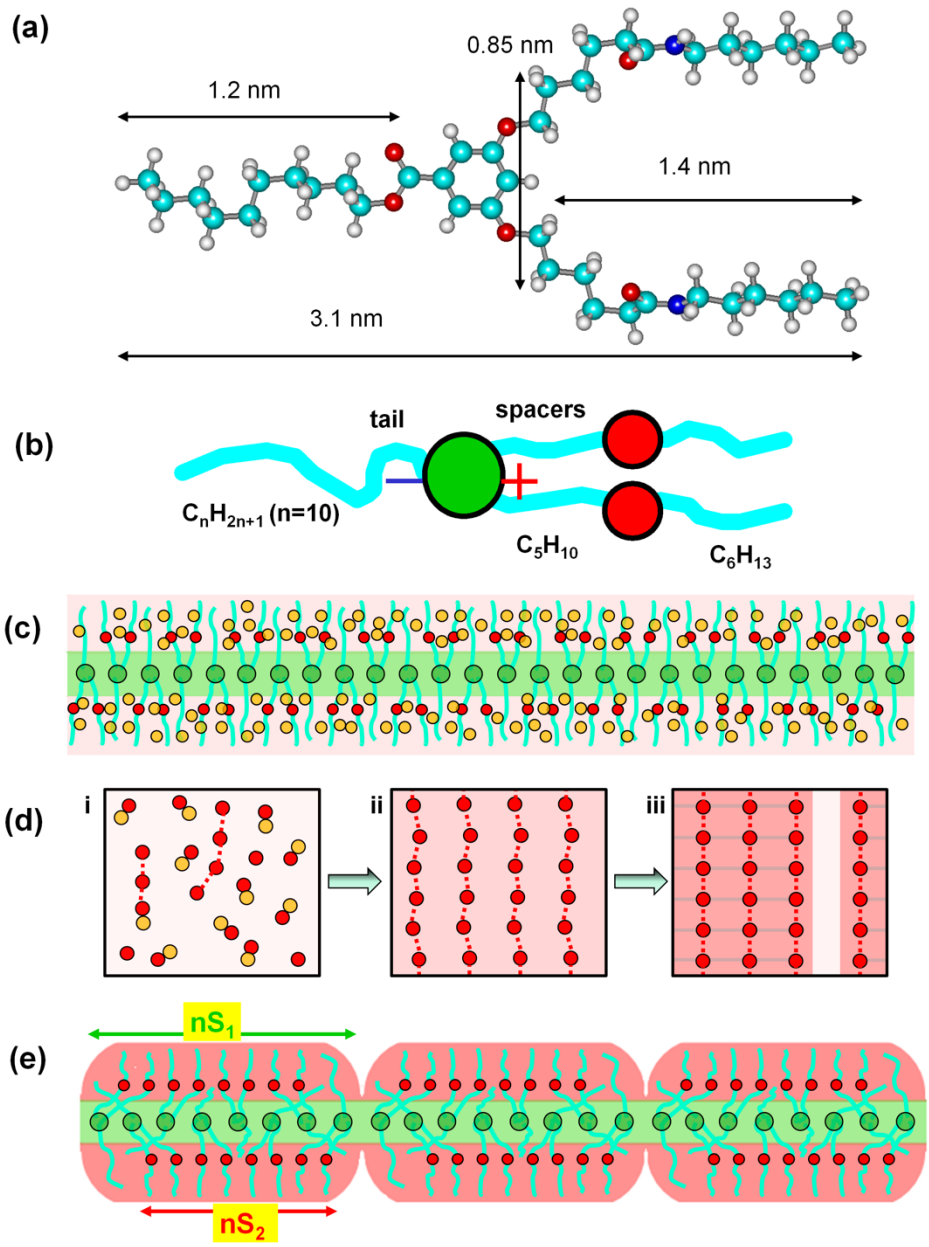

Fig. 5 (a) Chemical structure of the elongated conformation of a BPHB-10 molecule and (b) its cartoon showing the orientation of the dipole on the aromatic-ester ring (shown as green circle). (c) – (e) Principle kinetic stages of 'drying crack pattern' formation (within a BHPB-10 monolayer) during the drop casting from cyclohexanone solution: (c) Side view of semi-dried continuous lamellar layer where the ring SIGs are arranged into 2D continuous sublayer, while the amide SIGs are solvated by cyclohexanone (yellow

circles) and hence are not ordered (SIGs are shown as in Fig. 2e). (d) Top view (amide 2D-sublayer only) of the same layer as in (c) during the solvent evaporation: i) de-solvation of amide SIGs causes their association, this results into H-bound reversible chain formation; ii) amide SIGs are 'polymerized' but amorphous; iii) crystallization and thereby induced shrinking of the amide sublayer. H-bonds causing 'polymerization' are indicated by red dotted lines, sidewise inter-amide attractions are indicated by grey lines, the crack between nanoribbons is shown by the pale region. (e) The same layer as in (c), but after complete drying, i.e., removal of cyclohexanone. Here, the continuous monolayer is "broken up" into parallel nanoribbons of a characteristic width because of the specific area difference between the aromatic (S1) and the amide (S2) sub-layers.

The height (h_l) of the lamella (Fig. 5c) should roughly correspond to the long axis of the elongated BHPB-10 molecule $h_{mol} \sim 3.1$ nm (Fig. 5a); h_l should also be similar to the thickness of the sandwich structure in the curved lamella shown in Fig. 2e, which (based on the SANS measurements shown in ref. 49) was estimated to be $h_{tub} \sim 3.4$-3.5 nm. If the drop casted amount of BHPB-10 molecules is higher than the one required for forming a single lamellar monolayer, a multi-lamellar structure, i.e., a stack of several such lamellae, is formed. In a dry single lamella of thickness h, the specific area per one molecule can be calculated as $S_l = \mu/(N_A \rho h) \sim 0.33$-$0.37$ nm^2 where μ is the molar mass of BHPB-10 (μ = 689 g), ρ its density (estimated at $\approx$ 1 g/ml), $N_A = 6.023 \times 10^{23}$ molecules/mole and the range of values of thickness $h \sim 3.1$-3.5 nm as mentioned above. Both types of lamellae (symmetric, Fig. 5c, and asymmetric sandwich, Fig. 2e) have

similar values of h and S_1. The values of S_1 are also close to the result of Amber modeling[61] of the molecule for the 2D aromatic-ester ring monolayer at zero temperature: S_0= 0.32 nm^2 (see Fig. S-7 and S-8 in ESM). We estimate now the bulk concentration c_{sing} of BPHB-10 in the solution which corresponds to a complete monolayer lamella (Fig. 5c) formed via drop casting (for the initial thickness of the drop film, d_{dc} = 50 μm): $c_{sing} = \rho h/d_{dc} \sim 0.07$ mg/ml. Our observation of a film consisting of 2-3 layers deposited from c = 0.2 mg/ml (cf. Fig. 4c,d) is consistent with this value of c_{sing}.

After initial lamella formation (Fig. 5c), the systems comes to the final stage of the drying process, when almost no cyclohexanone molecules are left in the deposited film. The amide groups start to mutually attract each other and 'chains' of H-bound amide groups are formed (Fig. 5d(i)). Initially, these amide 'chains' are weakly ordered (see Fig. 5d(ii)), but they laterally attract each other via van der Waals and dipole attraction forces. Hence, a 2D crystalline sub-layer of chains made of H-bound amide groups is energetically most favorable. The ordering of the amide chains leads to a lateral shrinking of the amide sub-layer (Fig. 5d(iii)), such shrinkage, in turn, causes an area mismatch between the ring and the amide sub-layers. The mismatch is characterized by the difference in respective specific (per one BHPB molecule) areas S_1 and S_2 of these two SIG-stabilized sub-layers ($S_1 > S_2$), and hence it may result in the formation of a 'desiccation crack pattern',[67,68] Fig. 5e (note that the SIGs in these two sub-layers (green and red) are connected via short alkyl spacers C_5H_{10}). The cracking amide sub-layers are characterized by a strong asymmetry: H-bonds between amide SIGs are substantially stronger than other attractions between them, hence the amide sub-layers crack in their weak direction (the crack lines should be parallel to the chains of H-bonds, in order to

preserve them, cf. Fig. 5d and Fig. S-9 in ESM and refer to minor longitudinal ripple structure of the stripes Fig.4). Thus, the final meso-pattern is ribbon-like.

The width w of the ribbons can be estimated via a scale analysis of the specific energy of the layer:

$$E = \gamma/w + 0.5\ \kappa\ (S_2\text{-}S_2^{(0)})^2 + \chi\ (S_1\text{-}S_2)^2\ w^2/12 \qquad (1)$$

where E is a layer energy per unit area, γ is a normalized edge energy of the ribbon, κ is the normalized elastic constant of the amid layer, S_2 and $S_2^{(0)}$ are specific areas for the mismatch-stretched and the relaxed (free) amide layers, respectively, $S_2^{(0)} < S_2 < S_1$, and χ is the elastic constant related to alkyl spacer deformations. For simplicity of the analysis, we assumed that the quasi-2D sub-layer of aromatic rings is solid-like and hence incompressible (the rings are oriented perpendicular to the plane of the layer). By contrast, the amide layer is considered to be deformable, e.g., by tilting of the amide groups via their rotation around the lines formed by H-bonds (i.e. for the amide layer shown in Fig. 5d(iii), it is stretching in horizontal direction).

If the mismatch between specific areas in the dried ring and amide sub-layers stays below a critical value (δS_{cr}), i.e. if

$$(S_1\text{-}S_2^{(0)}) < \delta S_{cr} \equiv 2\ (\ \gamma^2\chi\ /\ 6\kappa^3\ )^{1/4} \qquad (2)$$

no 'drying crack pattern' will be formed. There, the energy for forming edges is too costly and thus prevents a splitting of the lamella into ribbons. For the opposite case, i.e. if $(S_1\text{-}S_2^{(0)}) > \delta S_{cr}$, cracking is possible, the ribbon pattern is more favorable than the stretched compact lamella. For the critical situation, i.e. if $(S_1\text{-}S_2^{(0)}) = \delta S_{cr}$, a characteristic

value of the width (w^*) of the nanoribbons is obtained:

$$w^* \sim (6\kappa/\chi)^{1/2} \quad (3)$$

In the limit of $(S_1\text{-}S_2^{(0)}) >> \delta S_{cr}$, the energy (Eq. 1) is minimal for ribbons of the width

$$w^* \sim (6\,\gamma / \chi(S_1\text{-}S_2^{(0)})^2)^{1/3} \quad (4)$$

These predictions explain why nanoribbons were observed in the experiments and why they had a rather well-defined, characteristic width (cf. Fig. 4). By the estimations (see section S-6 of the ESM) of the material constants from eq. (4), one can conclude that typical ribbon width is around w*~12 nm, which is close to the experimental values of Fig. 4. It is interesting to note that the width eq. (4) was independent of the nature of the substrate: on Si wafer (Fig. 4a), on carbon coated grid (Fig. 4e) and on the top of BHPB lamella (Fig. 4b) similar ribbon widths are emerged. The formation of crack patterns is a first order transition, hence, as a signature of hysteresis, some fluctuations in the width of the nanoribbons can be expected, as seen in the micrographs. The drying process initially caused the formation of a crack pattern in the top-most layer (solvent evaporated from the surface of the sample). This initial pattern then guided orientation of the nanoribbons in the underlying layers (see Fig. 4c).

Switching between nanoribbons and nanotubes

Two morphologies (tubules and ribbons) can be formed from the same BHPB-10 molecules when they are deposited from different solutions onto wafers, Fig. 2 and 4. In order to study their stability and to exploit the possibility of switching between the

morphologies, we annealed already deposited nanoribbons in a favorable environment which could allow partial mobility for the molecules without dissolving them (TESVA method, see section "Experimental section").[56,57,69] Solvent vapor sops the surface aggregates, and the presence of solvent molecules in the layer and the increased temperature gives some mobility to BHPB-10 molecules and allow them to rearrange while keeping them in contact with the surface. As a result, the molecules adopt the configuration with the minimum free energy and hence form stable nanostructures. Apart from transformation between two distinctly different morphologies by dissolving the first one and forming (crystallizing) the second one, i.e., a process of re-crystallization, a change in the quality and in the nature of the solvent sometimes causes re-organization of molecules within already formed self-assembly structures, because changes in the solvent can affect interactions between the functional groups of deposited molecules.[55]

Along these concepts, we have annealed BPHB-10 nanoribbons, obtained by drop casting from cyclohexanone, in cyclohexane vapor, which is not expected to disturb the possibility of inter-amide H-bonding. As a result, at different annealing intervals we observed a slow transformation of deposited on the substrate from flat nanoribbons (~12 ± 4 nm wide) to twisted curved nanosheets with a width up to ~70 nm (Fig. 6) and eventually to nanotubes (Fig. 7) with a diameter of ~30 nm. Annealing in cyclohexane vapor for a relatively short time provided insight into the process of how nanoribbons transform into nanotubes (Fig. 6a,b). Different types of structures became visible in Fig. 6a. Some of the initial nanoribbons (labeled as R_1) with a width of ~10-14 nm still remained, some new nanoribbons (labeled as R_2) appeared and grew wider, attaining a width of ~25 nm, and some merged into even wider nanostructures (R_3). AFM showed an

increase in height as the width of the nanoribbons grew, indicating that these structures started to curve.

The observation of a change in morphology suggests that dry nanoribbons in Fig. 4 do not represent equilibrium structures. When BHPB-10 molecules gained mobility, due to the presence of weakly interacting solvent molecules, they started to rearrange and formed more stable curved structures. Under the conditions of TESVA, re-ordering of the molecules was a slow process as indicated by the fact that even after 30 minutes of annealing still some flat or only weakly twisted nanoribbons existed (Fig. 6). With increasing annealing time, the nanoribbons started to curl into helical nanoribbons. Moreover, both left and right-handed twisted nanoribbons of comparatively large width were found (Fig. 6b) in line with our expectation, that for achiral BHPB-10 molecules there is no preferred direction of twisting. The angle θ between the long axis of the helix and its edges was measured to be $\theta \sim 30 \pm 4°$ (Fig. 6c).

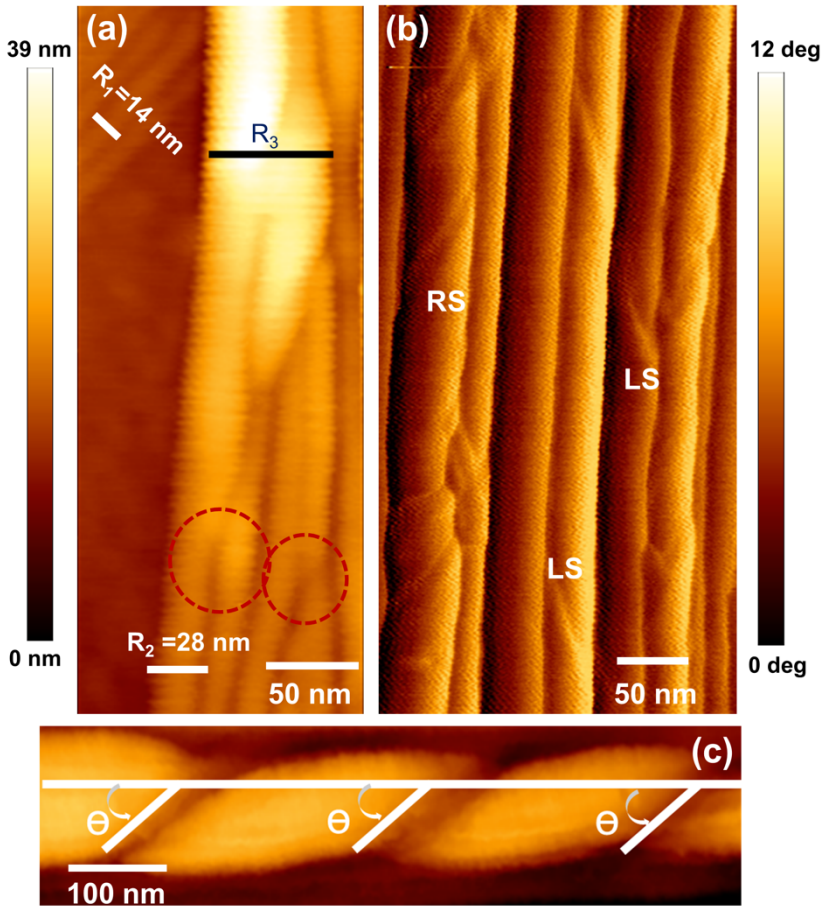

Fig. 6 AFM images of BHBP-10 dissolved in cyclohexanone (0.05 mg/ml), drop casted onto a Si substrate and then annealed in cyclohexane vapor at 60 °C. (a) Topographic image showing the transformation of nanoribbons (R_1) to wider nanoribbons (R_2) via merging (encircled regions), followed by a transformation into a wider and curved nanosheet (R_3). (b) Phase image showing both right and left handed helical nanoribbons, marked as RS and LS, respectively. (c) A helical nanoribbon showing the twist angles θ between the edges of the nanoribbon and its long axis, yielding $\theta \simeq 30 \pm 4°$. The annealing time for (a) and (b) was 30 minutes and for (c) it was 1 hour.

After 2 hours of annealing, fully formed nanotubes were observed (Fig. 7) with a diameter ~30 nm and a length up to several micrometers, similar to the ones formed directly in cyclohexane solutions (Fig. 2). It is quite understandable as, during the TESVA induced switching from nanoribbons to nanotubes, solvent molecules were present, generating solvent-mediated forces among BHPB-10 molecules. Probably driven by van der Waals and by capillary forces, the nanotubes align and form bundles (Fig. 7). Such bundles of nanotubes, also observed in bulk solution, most likely represent the equilibrium structure, as even after long annealing for 48 hours at 60 °C in cyclohexane vapor, no further changes in structure were observed.

Capillary forces were probably also at the origin of metastable wide aggregates observed on Fig. 6a (nanosheets R_3). There, interfacial tensions acted against a detachment of nanostructures from the surface, and thus against helix formation. Indeed, the equilibrium helix diameter of ca. 30 nm (see Fig. 7) is significantly larger than the thickness of an adsorbed monolayer of BHPB-10 swollen by some solvent molecules, which formed during TESVA due to condensation of cyclohexane molecules on BHPB-10 structures.

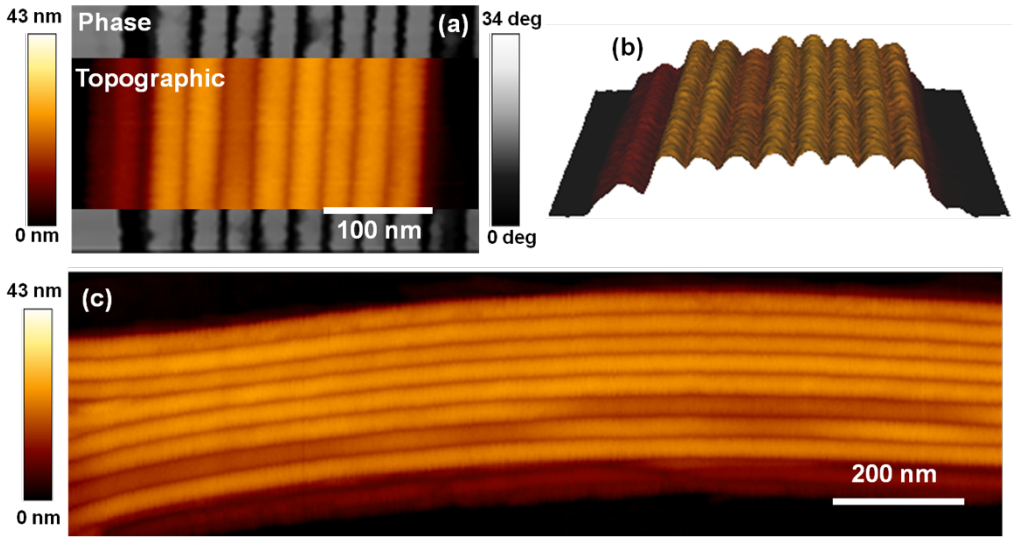

Fig. 7 AFM (a) combined topographic and phase image and (b) 3D image of BHBP-10 dissolved in cyclohexanone (0.05 mg/ml), drop casted on Si substrate and then annealed in cyclohexane vapor at 60 °C for 2 hours. The nanotubes have a diameter of ~30 nm and a length up to several micrometers (c).

The observed transformation from flat nanoribbons to nanotubes reflects the difference between the two solvents. Cyclohexanone, because of its polarity and its H-acceptor character, strongly interacts with BHPB-10, solvates amide groups and destroys H-bonds. As a result, flat lamellae with two equivalent sides (see Fig. 5) are formed, as only one type of SIGs is effectively left: The BHPB-10 molecules are linked only via π-stacked rings. By contrast, cyclohexane is apolar and does not disrupt specific interactions between SIGs of BHPB-10 molecules, hence two distinct types of SIGs (amides and rings) are at work simultaneously. This leads to the formation of mesostructures with non-equivalent sides, hence potentially curved (Fig. 2). Apparently, the inner structure, i.e., the arrangement of amide and aromatic sublayers with respect to each other, in the flat and the curved aggregates is different. On the one hand, in

aggregates derived from cyclohexane (as they are found in the bulk, or in the structures deposited on the surface, or in the final structures obtained by TESVA method in cyclohexane vapor), an asymmetric two sub-layer structure of SIGs (formed by amide groups and by the aromatic ester rings, respectively) causes curved sandwich lamellae (Fig. 2e,f). On the other hand, deposited from cyclohexanone, a more symmetric three sub-layer structure (formed by two layers of amide groups separated by a layer of aromatic ester rings) leads to flat nanoribbons (Fig. 5c). In the latter case, formation of the amide sub-layers is assumed to take place only at the very last stages of the drying process, while in the wet state, i.e., when cyclohexanone still solvates BHPB-10 molecules, only the central 'aromatic ester' sublayer (due π-stacking of rings) is present. A transformation between these two distinctly different morphologies is only possible by dissolving the first one and forming (crystallizing) the second one, i.e., a process of re-crystallization. Indeed, the initial (R_1) and the resulting (R_2, R_3) morphologies appear to be located randomly in Fig. 6a (while transformation from (R_2) to (R_3) looks like hereditary). Once a nucleus of the asymmetric structure (R_2) is formed, it can grow in size and can be transformed smoothly into (R_3) and then to a tubule (top part of Fig. 6a). All-atom models[61] demonstrate that for rings and amide groups connected by short C_5H_{10} spacers, a very limited range of rotation angles between the crystalline axes of the amide and ring sublayers are available, see Fig. S-10 in ESM. Although for each particular molecule (with an achiral chemical structure, Fig. 5a) such rotation can be in either direction, cooperative effects within an aggregate should cause that all BHPB-10 molecules rotate in the same direction. Thus, due to spontaneous symmetry breaking,[43] the resulting twisted structures should either be left- or right-handed (see Fig. 6b).

Via the exposure of nanotubes to cyclohexanone, we have also verified that the reverse process, switching nanotubes to nanoribbons, is also possible. Starting from a cyclohexane solution of BHPB-10, which contained nanotubes, we added the same amount of cyclohexanone to this solution. Cyclohexanone destroyed the H-bonds and the π-π interactions between BHPB-10, causing the disassembly of the nanotubes. Drop casting this cyclohexanone/cyclohexane solution onto the substrate led to the self-assembly of BHPB-10 molecules into nanoribbons, see Fig. S-3d in the ESM, which are identical to the nanoribbons of Fig. 4(as the cyclohexane evaporates first from the mixture, the last stages of drying of BHPB-10 solution in the mixed solvent are identical to the drying from pure cyclohexanone, cf. Fig. 5c,d). In particular, these new nanoribbons (Fig. S-3) could be transformed again into nanotubes (Fig. 8) by TESVA in cyclohexane vapor.

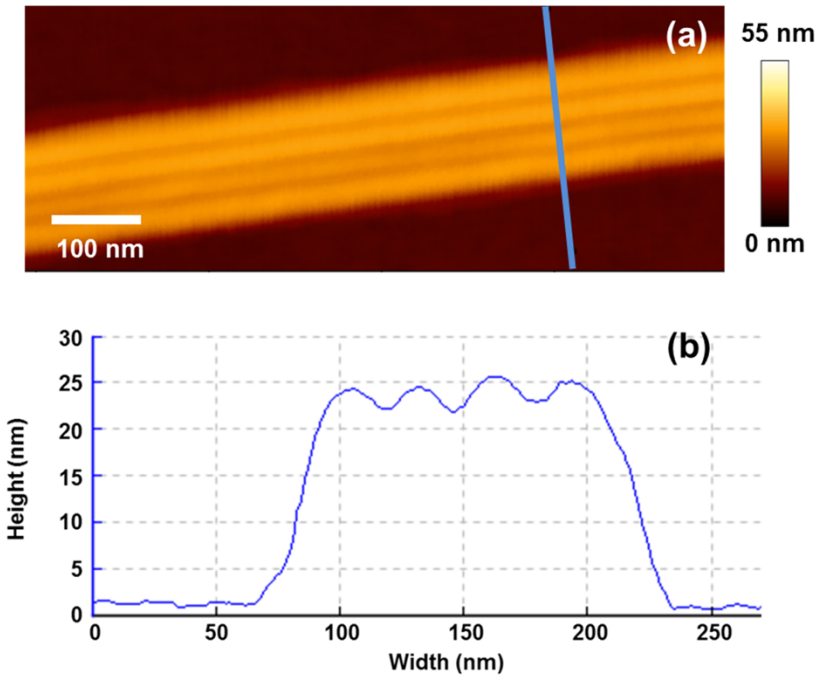

Fig. 8 AFM topographic (a) 2D and (b) height profile of nanotubes reformed from nanoribbons of BHPB-10 molecules on the substrate after annealing in the presence of

cyclohexane vapor.

After the transformation of a flat lamella (Fig. 9a) into a curved lamella (Fig. 9b,c), the shape of twisted nanoribbons comes from the presence of two favored directions in the two quasi-2D sub-layers forming the mesostructure. First, there is a direction of 'easy breakage' (preserving the H-bonds), which is in the direction parallel to the H-bonds in the amide sub-layer (see Fig. S-9 in ESM for details); this direction coincides with the nanoribbon edge (see the direction indicated by the red arrow in Fig. 9c). Second, there is a direction of 'easy bending', which keeps the aromatic rings parallel to each other (thus preserving the π-π interactions); this direction is indicated by the green arrow in Fig. 9c. It should be orthogonal to the axis of the future nanotube (cf. Fig. 9d-f) due to the geometry of the bent 2D-layer. The angle $\alpha \sim 60°$ between these two favored directions is determined by the energy of the inner rotations within the C_5H_{10} short alkyl spacers connecting the aromatic and the amides SIGs within the BHPB molecules (see Fig. S-10 in ESM for more details). The same angle α determines the helical shape of the growing tape. The strongest force for stabilization of the nanostructure originates from the H-bonds, which also define the direction of fastest growth of the nanostructure. Therefore, nanotube formation starts with the formation of long helical nanoribbons (Fig. 6b,c) driven by multiple H-bonding. Simultaneously with the growth in the H-bonding direction, the ordered sublayers also grow in the orthogonal direction, thus increasing the width (w) of the nanoribbon (Fig. 9d,e). When a nanoribbon gets wider, its sides start to touch each other in the course of twisting and hence fuse to a nanotube (Fig. 9f).

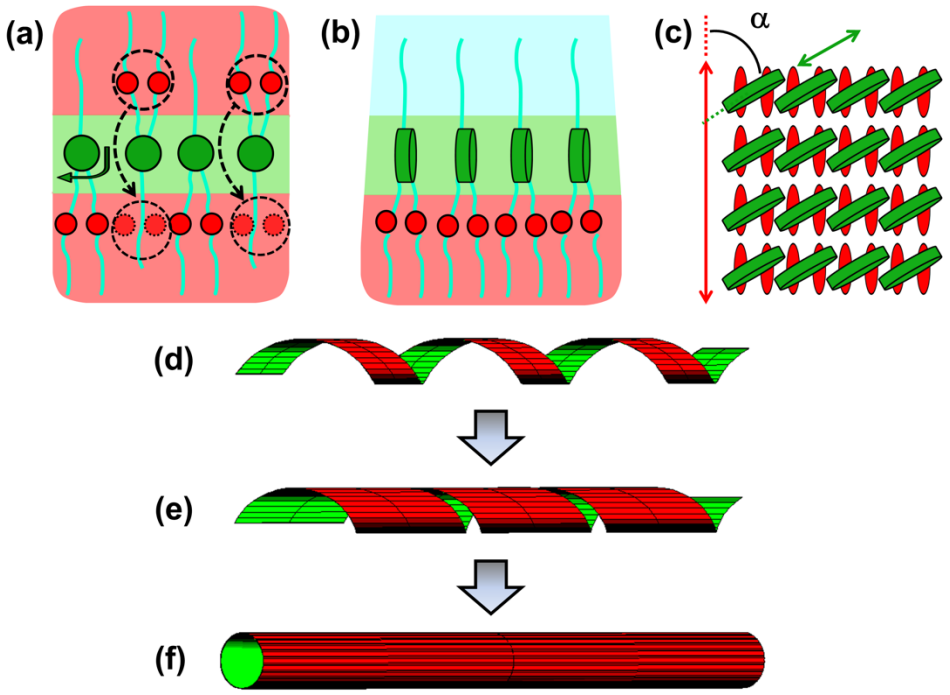

Fig. 9 On the switching of a flat to a curved lamella, which eventually transforms into a helical structure of achiral BHPB-10 molecules. The green disks represent the aromatic rings and the red ellipses the amide groups. (a) Schematic representation of the translation of amide groups induced by H-bonding and tilting of aromatic rings, transforming a flat lamella into a curved lamella. (b) Side view of quasi-2D crystalline amide and aromatic-ester sub-layers connected by short alkyl spacers in curved lamella. (c) Top view of (b) showing amide groups and aromatic rings: the planes of aromatic rings (green arrow) are tilted by an angle $\alpha \sim 60°$ relative to direction of H-bonds (red arrow). During formation, the nanoribbon grows fastest along the direction of the H-bonds and more slowly in the orthogonal direction. The latter growth process is responsible for widening of the nanoribbon d&e), leading eventually to the formation of nanotubes (f).

Conclusions

The interplay of H-bonding and π-π stacking interactions in solutions of achiral BHPB-10 molecules proved to be controllable via the use of appropriate solvents, thus leading to the formation of various self-assembled planar and curved nanostructures. In the presence of an inter-amide H-bond favoring solvent (cyclohexane), strong bonds between the amide groups also bring the aromatic rings closer together, favoring π-π interactions. These interactions generated a lamellar mesostructure based on a quasi-2D layer of aromatic-ester groups linked to a quasi-2D layer of amide groups. Symmetry breaking due to the differences in molecular cross-sections for these two sublayers together with the alkyl tails osmotic pressure causes a spontaneous curvature of the lamella, leading to the formation of nanotubes. Using a solvent suppressing the formation of H-bonds (cyclohexanone), a quasi-2D layer of π-stacked aromatic-ester rings, arranged in an antiparallel fashion, is formed, sandwiched between layers of loosely interacting amide groups. In the course of solvent evaporation, progressively accrued H-bonds are being established between the amide-groups, leading to the formation of two ordered quasi-2D amide layers. The formation (crystallization) of these H-bonded layers then induces stresses, which, in turn, lead to the formation of crack patterns in the flat lamellar trilayer structure, yielding nanoribbons of finite width. Enabling or disabling the formation of H-bonds via the presence of appropriate solvent molecules allowed us to tune the self-assembly process and to switch reversibly between nanoribbons and nanotubes. When a layer of aligned nanoribbons deposited onto a solid substrate was exposed to the vapor of a solvent favorable for the formation of inter-amide H-bonds, we observed structure

rearrangements leading to a transformation from planar to helical nanoribbons, which finally grew into nanotubes. On the contrary, exposing of these nanotubes to a solvent suppressing the formation of inter-amide H-bonds resulted in switching nanotubes back to nanoribbons.

Our findings provide insight in the interplay of complementary inter-molecular interactions for a profound understanding of self-assembly of achiral molecules into nanotubes and nanoribbons. Based on such understanding, we demonstrated an effective pathway to tailor morphologically different nanostructures from the same building unit by exploiting specific inter-molecular interactions. We also developed a specially-tailored TESVA method which allowed us to build perfectly-ordered, self-assembled tubular or ribbon-like structures on surfaces, highly monodisperse in width and with a length of dozen of micrometers.

Acknowledgments

The authors are very grateful to Alexander Semenov for very fruitful discussions to Marc Schmutz and Christian Blanck for the valuable help with TEM (all them from Institute Charles Sadron (ICS), Strasbourg, France). We acknowledge funding from the Deutsche Forschungsgemeinschaft (IRTG-1642 “Soft Matter Science”). The AFM images were obtained by the facilities of Experimental Polymer Physics group, Freiburg, Germany, and TEM images by the ICS microscopy facility.

Electronic Supplementary Material: Additional information on the experimental methods, solutions and deposit characterization and on details of modeling is available in the online version of this article at ……...

References

1 R. Thiruvengadathan, V. Korampally, A. Ghosh, N. Chanda, K. Gangopadhyay and S. Gangopadhyay, *Rep. Prog. Phys.*, 2013, **76**, 1–53.

2 C.-A. Palma, M. Cecchini and P. Samorì, *Chem. Soc. Rev.*, 2012, **41**, 3713–3730.

3 V. Berl, I. Huc, R. G. Khoury, M. J. Krische and J. M. Lehn, *Nature*, 2000, **407**, 720–723.

4 E. Gazit, *Chem. Soc. Rev.*, 2007, **36**, 1263–1269.

5 S. Zhang, *Nat. Biotechnol.*, 2003, **21**, 1171–1178.

6 T. G. Barclay, K. Constantopoulos and J. Matisons, *Chem. Rev.*, 2014, **114**, 10217–10291.

7 T. Shimizu, *Bull. Chem. Soc. Jpn.*, 2008, **81**, 1554–1566.

8 R. S. R. Min-Feng Yu, Oleg Lourie, Mark J. Dyer, Katerina Moloni, Thomas F. Kelly, *Science (80-.).*, 2000, **287**, 637–640.

9 S. Zhang, *Adv. Cancer Res.*, 2008, **99**, 335–362.

10 A. T. Bell, *Science*, 2003, **299**, 1688–1691.

11 N. B. Sopher, Z. R. Abrams, M. Reches, E. Gazit and Y. Hanein, *J. Micromechanics Microengineering*, 2007, **17**, 2360–2365.

12 J. C. Moghimi, S. M.; Hunter A. C.; Murray, *FASEB J.*, 2005, **19**, 311–330.

13 W. Lu and C. M. Lieber, *J. Phys. D. Appl. Phys.*, 2006, **39**, R387–R406.

14 M. G. Bawendi, M. L. Steigerwald and L. E. Brus, *Annu. Rev. Phys. Chem.*, 1990, **41**, 477–496.

15 P. J. Pauzauskie and P. Yang, *Mater. Today*, 2006, **9**, 36–45.

16 S. Werner, S. Marillonnet, G. Hause, V. Klimyuk and Y. Gleba, *Proc. Natl. Acad. Sci. U. S. A.*, 2006, **103**, 17678–17683.

17 C. M. Patolsky, F.; Zheng, G.; Lieber, *Anal. Chem.*, 2006, **78**, 4261–4269.

18 I. Willner, R. Baron and B. Willner, *Biosens. Bioelectron.*, 2007, **22**, 1841–1852.

19 W. Si, X.-B. Hu, X.-H. Liu, R. Fan, Z. Chen, L. Weng and J.-L. Hou, *Tetrahedron Lett.*, 2011, **52**, 2484–2487.

20 B. Gong and Z. Shao, *Acc. Chem. Res.*, 2013, **46**, 2856–2866.

21 E. Protopapa, S. Maude, A. Aggeli and A. Nelson, *Langmuir*, 2009, **25**, 3289–3296.

22 C. R. Martin, *Chem. Mater.*, 1996, **8**, 1739–1746.

23 E. Reches, M.; Gazit, *Science (80-.).*, 2003, **300**, 625–627.

24 L. A. Estroff and A. D. Hamilton, *Chem. Mater.*, 2001, **13**, 3227–3235.

25 E. Dujardin, C. Peet, G. Stubbs, J. N. Culver and S. Mann, *Nano Lett.*, 2003, **3**, 413–417.

26 D. S. Kim, R. Ji, H. J. Fan, F. Bertram, R. Scholz, A. Dadgar, K. Nielsch, A. Krost, J. Christen, U. Gösele and M. Zacharias, *Small*, 2007, **3**, 76–80.

27 C. Tarabout, S. Roux, F. Gobeaux, N. Fay, E. Pouget, C. Meriadec, M. Ligeti, D. Thomas, M. IJsselstijn, F. Besselievre, D.-A. Buisson, J.-M. Verbavatz, M. Petitjean, C. Valéry, L. Perrin, B. Rousseau, F. Artzner, M. Paternostre and J.-C. Cintrat, *Proc. Natl. Acad. Sci. U. S. A.*, 2011, **108**, 7679–7684.

28 H. Fenniri, B.-L. Deng, A. E. Ribbe, K. Hallenga, J. Jacob and P. Thiyagarajan, *Proc. Natl. Acad. Sci. U. S. A.*, 2002, **99 Suppl 2**, 6487–6492.
29 T. M. Chung, H. F. Wang, T. Lin, Y. W. Chiang, Y. C. Chen, B. T. Ko and R. M. Ho, *Macromolecules*, 2012, **45**, 9727–9733.
30 J. N. Israelachvili, D. J. Mitchell and B. W. Ninham, *J. Chem. Soc. Faraday Trans. 2*, 1976, **72**, 1525–1568.
31 J. V. Selinger, M. S. Spector and J. M. Schnur, *J. Phys. Chem. B*, 2001, **105**, 7157–7169.
32 T. Kunitake, Y. Okahata, M. Shimomura, S. Yasunami and K. Takarabe, *J. Am. Chem. Soc.*, 1981, 5401–5413.
33 J. H. Jung, S.-H. Lee, J. S. Yoo, K. Yoshida, T. Shimizu and S. Shinkai, *Chem. - A Eur. J.*, 2003, **9**, 5307–5313.
34 Y.-W. Chiang, R.-M. Ho, C. Burger and H. Hasegawa, *Soft Matter*, 2011, **7**, 9797–9803.
35 A. Brizard, R. Oda and I. Huc, *Top. Curr. Chem.*, 2005, **256**, 167–218.
36 R.-M. Ho, Y.-W. Chiang, S.-C. Lin and C.-K. Chen, *Prog. Polym. Sci.*, 2011, **36**, 376–453.
37 R. Oda, F. Artzner, M. Laguerre and I. Huc, *J. Am. Chem. Soc.*, 2008, **130**, 14705–14712.
38 A. Singh, P. E. Schoen and J. M. Schnur, *J. Chem. Soc. Chem. Commun.*, 1988, 1222–1223.
39 A. Aggeli, I. A. Nyrkova, M. Bell, R. Harding, L. Carrick, T. C. McLeish, A. N. Semenov and N. Boden, *Proc. Natl. Acad. Sci. U. S. A.*, 2001, **98**, 11857–11862.
40 Y. Wang, D. Zhou, H. Li, R. Li, Y. Zhong, X. Sun and X. Sun, *J. Mater. Chem. C*, 2014, **2**, 6402–6409.
41 J. Kim, J. Lee, W. Y. Kim, H. Kim, S. Lee, H. C. Lee, Y. S. Lee, M. Seo and S. Y. Kim, *Nat. Commun.*, 2015, **6**, article 6959.
42 Anuradha, D. D. La, M. Al Kobaisi and S. V. Bhosale, *Sci. Rep.*, 2015, **5**, article 15652.
43 R. F. B. and C. M. K. Jonathan V. Selinger, Zhen-Gang Wang, *Phys Rev Lett.*, 1993, **70**, 1139–1142.
44 S. Wang, Y. Zhang, Y. Xia and B. Song, *Nanoscale*, 2015, **7**, 17848–17854.
45 S. Pakhomov, R. P. Hammer, B. K. Mishra and B. N. Thomas, *Proc. Natl. Acad. Sci. U. S. A.*, 2003, **100**, 3040–3042.
46 S.-T. Wu, Y.-R. Wu, Q.-Q. Kang, H. Zhang, L.-S. Long, Z. Zheng, R.-B. Huang and L.-S. Zheng, *Angew. Chem. Int. Ed. Engl.*, 2007, **46**, 8475–8479.
47 J. M. Ribó, J. Crusats, F. Sagués, J. Claret and R. Rubires, *Science*, 2001, **292**, 2063–2066.
48 W. Yang, X. Chai, L. Chi, X. Liu, Y. Cao, R. Lu, Y. Jiang, X. Tang, H. Fuchs and T. Li, *Chem. - A Eur. J.*, 1999, **5**, 1144–1149.
49 F.-X. Simon, T. T. T. Nguyen, N. Díaz, M. Schmutz, B. Demé, J. Jestin, J. Combet and P. J. Mésini, *Soft Matter*, 2013, **9**, 8483–8493.
50 N. Díaz, F.-X. Simon, M. Schmutz, M. Rawiso, G. Decher, J. Jestin and P. J. Mésini, *Angew. Chem. Int. Ed. Engl.*, 2005, **44**, 3260–3264.
51 T. Ge and M. Rubinstein, *Macromolecules*, 2015, **48**, 3788–3801.
52 M. Rubinstein and A. N. Semenov, *Macromolecules*, 2001, **34**, 1058–1068.

53 A. N. Semenov, I. A. Nyrkova and A. R. Khokhlov, *Macromolecules*, 1995, **28**, 7491–7500.
54 C. Weber, T. Liebig, M. Gensler, A. Zykov, L. Pithan, J. P. Rabe, S. Hecht, D. Bléger and S. Kowarik, *Sci. Rep.*, 2016, 1–8.
55 M. A. Chavis, D. M. Smilgies, U. B. Wiesner and C. K. Ober, *Adv. Funct. Mater.*, 2015, **25**, 3057–3065.
56 K. Jahanshahi, I. Botiz, R. Reiter, H. Scherer and G. Reiter, *Cryst. Growth Des.*, 2013, **13**, 4490–4494.
57 E. Treossi, A. Liscio, X. Feng, V. Palermo, K. Müllen and P. Samorì, *Small*, 2009, **5**, 112–119.
58 C. A. Schneider, W. S. Rasband and K. W. Eliceiri, *Nat. Methods*, 2012, **9**, 671–675.
59 I. A. Nyrkova, A. R. Khokhlov and M. Doi, *Macromolecules*, 1993, **26**, 3601–3610.
60 A. K. Maerz, D. A. Fowler, A. V. Mossine, M. Mistry, H. Kumari, C. L. Barnes, C. A. Deakyne and J. L. Atwood, *New J. Chem.*, 2011, **35**, 784–787.
61 Private communication with Prof. Alexander Semenov, Institute Charles Sadron, Strasbourg, France 2014.
62 S. Whitelam, *Adv. Mater.*, 2015, **27**, 5720–5725.
63 F. Klappenberger, M. E. Canas-Ventura, S. Clair, S. Pons, U. Schlickum, Z. R. Qu, T. Strunskus, A. Comisso, C. Wöll, H. Brune, K. Kern, A. De Vita, M. Ruben and J. V. Barth, *ChemPhysChem*, 2008, **9**, 2522–2530.
64 R. Otero, J. M. Gallego, A. L. V. de Parga, N. Martín and R. Miranda, *Adv. Mater.*, 2011, **23**, 5148–5176.
65 C. A. Hunter and J. K. M. Sanders, *J. Am. Chem. Soc.*, 1990, **112**, 5525–5534.
66 S. L. Cockroft, C. A. Hunter, K. R. Lawson, J. Perkins and C. J. Urch, *J. Am. Chem. Soc.*, 2005, **127**, 8594–8595.
67 H. Colina and S. Roux, *Eur. Phys. J. E*, 2000, **1**, 189–194.
68 G. Gauthier, V. Lazarus and L. Pauchard, *Langmuir*, 2007, **23**, 4715–4718.
69 B. Spingler, S. Schnidrig, T. Todorova and F. Wild, *CrystEngComm*, 2012, **14**, 751–757.